A nonlinear analytical model for tensile failure prediction of pseudo-ductile composite laminates

A Nonlinear Analytical Model for Tensile Failure Prediction of Pseudo-Ductile Composite Laminates

Huabo Xiang[1,2], Yinxiao Zhang[2,3], Yang Chen[1,3,4*], Alfonso Pagani[5], Chao Zhang[2,3,4*]

[1] Yangtze River Delta ReseaIch Institute, Northwestern Polytechnical University, Taicang, 215400, China

[2] School of Aeronautics, Northwestern Polytechnical University, Xi'an, 710072, China

[3] Joint International Research Laboratory of Impact Dynamics and its Engineering Applications, Northwestern Polytechnical University, Xi'an, 710072, China

[4] School of Civil Aviation, Northwestern Polytechnical University, Xi'an, 710072, China

[5] Department of Mechanical and Aerospace Engineering, Politecnico di Torino, Torino, 10129, Italy

Abstract

In this paper, tensile nonlinear responses of composite laminates with $[\pm\theta_n]_s$ and $[\pm\theta_n/0]_s$ layups are investigated theoretically and experimentally. An analytical model, which integrates the progressive failure, shear nonlinearity, fiber rotation and fragmentation mechanism, is established to characterize the nonlinear tensile behaviors for the laminates. In the analytical model, a nonlinear factor is employed to describe the shear nonlinearity of the resin matrix, and it is governed by the shear stress. While for the progressive damage indexes, they are determined by the normal stresses. The degrees of the fiber rotation and fragmentation between layers are analytically formulated. Tensile tests are conducted and some experimental data from the literatures are also selected to verify the prediction accuracy of the analytical model. The findings reveal that the proposed analytical model can offer acceptably well predictions on the nonlinear behaviors for both pure fiber and hybrid fiber laminates. Then, the sensitivity analysis of the model parameters on the mechanical behaviors is carried out. The results show that the dominantly sensitive model parameter changes from E_1 to G_{12}, and finally to E_2 as the layering angle increases from 0° to 90°.

Keywords: Tensile nonlinear analytical model, shear nonlinearity, fiber rotation, progressive damage, composite laminates

1 Introduction

Continuous fiber-reinforced composite laminates exhibit the great advantages of lightweight structure, high specific strength, and high specific stiffness, and are thus widely used in the aerospace industry. However, their brittleness limits the reliability design and structural lightweight design. To overcome this drawback, design of nonlinear response, also called as pseudo ductility, is proposed and subsequently studied by many researchers. Fuller [1] first defined the pseudo ductility strain, as the failure strain minus the strain that is computed based on the same stress and the initial modulus.

The nonlinearity can arise from the influences on damage mechanism of hybrids effect [2-5], discontinuous fiber structure [6,7], nonlinear interfaces between tapes [8] and thin-ply method [9-20]. Moreover, fragmentation of middle layers [10-14], stable delamination [15-20] and fiber rotation [9, 21] are the mostly common studied accessible damage mechanisms, which are governed by the fiber types [22], the absolute or relative thickness of the layer [14, 17, 18], the angle of the fiber to the loading direction [11, 16-18, 20], and the stacking order [15, 17, 18]. Hassani et al. [14] found that the decrease of stress in tensile test relates to the thickness of the middle layer trough examining the effect of fiber volume fraction on mechanical properties of laminates. The smaller the thickness per unit area of the middle layer, the more conducive to fragmentation failure, to achieve a stable pseudo-ductility. Fotouhi et al. [11] studied the pseudo-ductile behavior for laminates under off-axis loads and found that the pseudo-ductility strain and maximum stress decrease with increasing off-axial angle. In addition, rising matrix cracking damage can be observed with the increase of the loading off-axial angle. Selezneva et al. [15] concluded that the brittleness is caused by the concentrated local damage, while the pseudo-ductility results from the dispersed and diverse damages consisting of fragmentation failure, fiber matrix degumming, matrix fracture, etc. Moreover, because of the randomness of damage, the higher dispersion degree leads to hinder the expansion of local damage.

Employing one or more damage mechanisms to achieve the nonlinear behaviors of laminates have attracted more attention to achieve easy production and wide application. As for the mostly commonly used $[\pm\theta_n/0]_s$ thin layer angle-ply laminates, the most probable failure mode for nonlinear response is demonstrated by the experiments conducted by Yu et al [10], Fotouhi et al [11], Czé [12] and Fuller et al [16]. It is found that the nonlinearity is caused by the fragmentation of the central layers

and brittle break of angle layers. They also found that the strength of the central layers of the laminate is increased compared to the behaviors of the corresponding single layer, because of the in-situ effect. For the simplified $[\pm\theta_n]_s$ laminates, Pozegic et al. [23] discovered that well rotated fiber in tensile test achieves better nonlinearity. Jalalvand et al. [17] and Fotouhi et al. [18] found that the delamination suppresion of $[\pm\theta]$ ply structure also leads to nonlinearity through the tensile experiments.

Apart from the above qualitative studies, three classical analytical models are built by Fuller et al. [1], Yuan et al. [9], and Jalalvand et al. [24-25] to characterize the nonlinear mechanical response for the laminates with $[\pm\theta_n]_s$ or $[\pm\theta_n/0]_s$ layup. Yuan et al. [9] obtained good prediction for the $[\pm30_4]_s$ laminates with difference fiber weight by considering the nonlinearity of the resin matrix [26] and fiber rotation. In their model, the fiber rotation obtained by the Digital Image Correlation (DIC) system. A theoretical method for fiber rotating calculation is also given by Fuller et al. [1]. While it does not show high accuracy on the prediction of mechanical response. Jalalvand et al. [24-25] established an analytical model for $[\pm\theta_n/0]_s$ laminates based on the classical laminate theory and rule of mixture. However, the stiffness nonlinearity for the laminates before the first fiber break is not considered causing some errors in stiffness prediction. The fiber rotation of angle-ply layers is also not considered.

In this paper, a new analytical model is established to characterize the tensile nonlinear response for the laminates with $[\pm\theta_n]_s$ and $[\pm\theta_n/0]_s$ layups in section 2. This analytical model integrates the shear nonlinearity, fragmentation mechanism, progressive failure and fiber rotation, so it combines the advantages of the precious research works and overcomes their shortcomings, like the data dependency, calculation efficient and precision. The delamination is not included in this model because of its unresolvable property [17,18]. In section 3, tensile tests are carried out to validate the prediction accuracy of the analytical model, and some experimental data from the literature are also utilized for validating. The sensitivity analysis of the model parameters is conducted in section 4 to explore their effects on the mechanical behaviors. Finally, a brief conclusion is given in section 5.

2 Form of analytical model

In the analytical model, it is assumed that the nonlinearity for the thin ply laminates with $[\pm\theta_n]_s$ and $[\pm\theta_n/0]_s$ layups comes from the fiber rotation of $\pm\theta^\circ$ layers, fiber fragmentation of 0° layer, progressive failure of matrix and fiber and completely failure of "overall" layers. The thickness effect and the hybrid effect are omitted, for

their negligible effect in these kinds of laminates.

Fig. 1 shows the flow chart for the theoretically modeling. The blue circle is the main calculation process to updated the global strain and stress of the laminates, while the red circle is to update the stiffness matrix of each layer.

In the blue circle, strains and stresses for the whole laminate and each layer under the global and local coordinates are computed, showing in section 2.1. Two failure criteria are employed to determine whether the laminate is totally failed, exhibiting in section 2.6.

In the red circle, the nonlinear behaviors of each layer are computed based on the stiffness degradation, governed by four mechanisms. In the green dotted box, the mechanism of fiber rotation is introduced to update the fiber angle, which is presented in section 2.2. In the orange, violet and yellow dotted boxes, the shear nonlinear model, progressive failure behavior and fragmentation mechanism are employed to further nonlinearized the stress-strain relation and presented in section 2.3-2.5, respectively. All of these four mechanisms, are computed based on strain and stress obtained in blue circle (i.e., the global strain and stress).

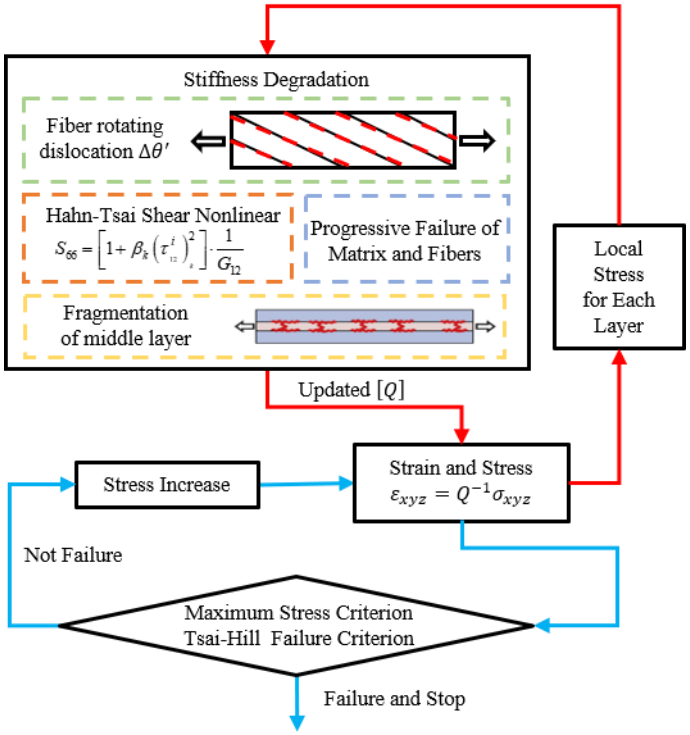

Fig. 1. Flow chart for the nonlinear analytical model

2.1 Meso-representative unit

Generally, a meso-representative unit should be small enough to be regarded as a

material point compared to the composite structure, while it should also be large enough to include the dominated microstructure features as possible, in order to describe the macroscopic equivalent properties of the laminates. In addition, if the microstructure is periodic, the size of the representative unit can be further reduced based on symmetry. In this study, the research objects are $[\pm\theta_n]_s$ and $[\pm\theta_n/0]_s$ laminates, which are symmetrical in the thickness direction. The fibers are assumed to be linearly elastic and isotropic, and they are arranged regularly in the matrix. While, the matrix is postulated to be uniform, linearly elastic and isotropic. The fiber and the matrix are perfectly bonded with no gaps. Based on these feature, a periodic representative volume unit is selected as shown in Fig. 2 (a). The A_+ and A_- denote $+\theta$ and $-\theta$ layers, respectively, which are regarded as homogeneous and transversely isotropic. The compliance matrix of these layers can be characterized using four in-plane engineering constants (i.e., E_1, E_2, v_{12}, and G_{12}) as

$$S_{11}=\frac{1}{E_1}, S_{12}=S_{21}=-\frac{v_{12}}{E_1}, S_{22}=\frac{1}{E_2}, S_{66}=\frac{1}{G_{12}} \tag{1}$$

The *C* layer corresponds to 0° plies in the $[\pm\theta_n/0]_s$ laminates or matrix in the $[\pm\theta_n]_s$ laminates. It is assumed to be homogeneous and transversely isotropic for the 0° plies and homogeneous and isotropic for the matrix. Thus, we have $S_{11}=S_{22}$ for the matrix, determined by the E_1, v_{12}, and G_{12}.

We assume that the *x*-*y* coordinate system represents the global coordinate system, in which the *x*-direction is the length direction of the laminate. The 1-2 coordinate system denotes the local coordinate system, where the 1-direction is the fiber direction. If the angle between the global and local coordinate systems are θ, as shown in Fig. 2 (b), the stress transform matrix is then given by

$$T=\begin{bmatrix} \cos^2\theta & \sin^2\theta & 2\sin\theta\cos\theta \\ \sin^2\theta & \cos^2\theta & -2\sin\theta\cos\theta \\ -\sin\theta\cos\theta & \sin\theta\cos\theta & \cos^2\theta-\sin^2\theta \end{bmatrix} \tag{2}$$

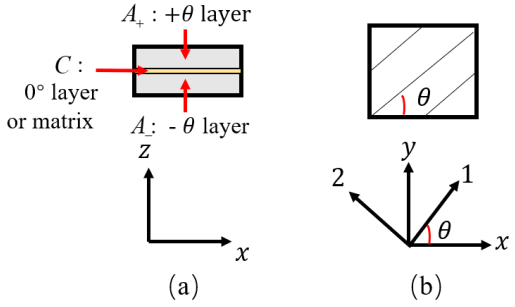

Fig. 2 (a) The schematic diagram of meso-representative unit, (b) the relation of *x*-*y* (global) coordinate system and 1-2 (local) coordinate system.

The relation of the compliance matrix of each layer in the global coordinate ($[\bar{S}]$) and local coordinate ($[S]$) is obtained by

$$\left[\bar{S}\right]_k = \left[T_k\right]^T \left[S\right]_k \left[T_k\right] \tag{3}$$

where the subscript $k = A_+,\ C$ and A_- accounts for the layer-type. According to the classical laminate theory, the stiffness matrix of the laminate can be computed by

$$Q = \frac{1}{t_{total}} \left\{ \left[\bar{S}\right]_{A_+}^{-1} t_{A_+} + \left[\bar{S}\right]_C^{-1} t_C + \left[\bar{S}\right]_{A_-}^{-1} t_{A_-} \right\} \tag{4}$$

Where t is the thickness for $A_+,\ C$ and A_- layers.

2.2 Fiber rotation

This section concerns the stiffness change caused by fiber rotation of the A_+ and A_- layers. The fibers are treated as inextensible and modelled as rotating towards the loading direction. Thus, fiber rotation acts as a 'scissoring', as described in [19, 27, 28]. The 'rotated' fiber angle, θ, is computed by

$$\theta = \arctan\left(\frac{\tan\theta_0 + \varepsilon_y}{1 + \varepsilon_x} \right) \tag{5}$$

where ε_x and ε_y are the longitudinal and transverse strains, respectively, and θ_0 is the original ply angle. Macroscopically, the fiber rotation will lead to a slight increase for the laminate stiffness if no damage occurs.

2.3 Shear nonlinearity

The shear nonlinearity of the resin matrix in each layer is considered to further capture the nonlinear behaviors of the laminate. Based on the Hahn and Tsai [26], the nonlinear stress-strain relationship can be given by

$$\begin{bmatrix} \varepsilon_1 \\ \varepsilon_2 \\ \gamma_{12} \end{bmatrix}_k = \begin{bmatrix} S_{11} & S_{12} & 0 \\ S_{12} & S_{22} & 0 \\ 0 & 0 & \left(S_{66}\right)\left[1 + \beta_k \left(\tau_{12}\right)_k^2\right] \end{bmatrix}_k \begin{bmatrix} \sigma_1 \\ \sigma_2 \\ \tau_{12} \end{bmatrix}_k \tag{6}$$

where, β_k is a nonlinear factor of the resin matrix, and τ_{12} is the in-plane local shear stress. For the laminates with $[\pm\theta_n]_s$ layup, the β_k is different for the A_+/A_- layer and the resin matrix layer, because the resin matrix layer is uniform, while the A_+/A_- layer is discontinued. However, for the laminates with $[\pm\theta_n/0]_s$ layup, the 0° layer

has the same value of β_k as the A_+ and A_- layers. In addition, the nonlinear factor for the interface among layers is ignored for its slight influence on the stiffness, which will be elaborated in the parameter sensitivity analysis of section 4.

2.4 Progressive failure

Because the fiber rotation and the shear nonlinearity do not completely reflect the stiffness change, the progressive failure is established to further describe the nonlinear behaviors of the laminates in this section. In this study, the theory of progressive failure is employed to determine the damage degree, and the Hashin criterion [29] and the criterion of Hu et al. [30-32] are combined to describe the failure behaviors. Therefore, the failure behaviors for the fiber and matrix of the laminate under the two-dimensional plane stress state are considered separately. For the fiber tension and compression, the damage indexes are given by

$$e_f = \begin{cases} \left(\frac{\sigma_{11}}{X_t}\right)^2 + \left(\frac{\sigma_{12}}{S}\right)^2, \sigma_{11} > 0 \\ \left(\frac{\sigma_{11}}{X_c}\right)^2, \sigma_{11} < 0 \end{cases} \tag{7}$$

While for the matrix tension and compression, the damage indexes are determined by

$$e_m = \begin{cases} \left(\frac{\sigma_{22}}{Y_t}\right)^2 + \left(\frac{\tau_{12}}{S}\right)^2, \sigma_{22} > 0 \\ \left(\frac{\sigma_{22}}{Y_c}\right)\left[\left(\frac{Y_c}{2S_{23}}\right)^2 - 1\right] + \left(\frac{\sigma_{22}}{S_{23}}\right)^2 + \left(\frac{\tau_{12}}{S}\right)^2, \sigma_{22} < 0 \end{cases} \tag{8}$$

Here, X_t and X_c are the tensile and compressive strengths in fiber direction, Y_t and Y_c denote the tensile and compressive strengths in transverse direction, and S is the in-plane shear strength.

Based on the damage indexes, the internal variables d_j can be defined to describe the stiffness attenuation of each layer, which is formulated by

$$d_j = min(1, e_j),\ j = f, m \tag{9}$$

where the subscript $j = f$ and m indicates the fiber and matrix, respectively. The elastic constants after damage are updated by

$$\begin{bmatrix} E_1 \\ E_2 \\ G_{12} \end{bmatrix}_{new} = \begin{bmatrix} 1 - F_{11} & 0 & 0 \\ 0 & 1 - F_{22} & 0 \\ 0 & 0 & 1 - F_{33} \end{bmatrix} \begin{bmatrix} E_1 \\ E_2 \\ G_{12} \end{bmatrix}_{old} \tag{10}$$

In (10), the subscript “new” means the updated elastic constants and the “old” denotes

the corresponding undamaged values. The components of the diagonal matrix F are computed by

$$\begin{aligned} F_{11} &= \max\left(0, d_f\right) \\ F_{22} &= \max\left(0, d_f, d_m\right) \\ F_{33} &= \max\left(0, d_f, d_m\right) \end{aligned} \tag{11}$$

Therefore, if combining the fiber rotation, shear nonlinearity and progressive failure, the nonlinear response for the $[\pm\theta_n]_s$ laminates could be described synthetically. However, for the $[\pm\theta_n/0]_s$ laminates, another damage mode (i.e., fragmentation of 0° ply) should be further introduced to describe its nonlinear behaviors.

2.5 Fragmentation of 0° ply

For the $[\pm\theta_n/0]_s$ laminates, fracture of the central 0° ply will always occur firstly, followed by the multiple fracture, which will lead to the nonlinear tension response [10-12,16]. In this work, we assume the damage of the 0° ply is symmetric with respect to the mid-plane and is governed by the stress in the fiber direction. Once the stress in fiber direction exceeds 7/18 of the tensile strength of the middle layer, the first fracture in the 0° ply will occur, followed by the fragmentation. However, the transverse tensile strength and in-plane shear strength of a single layer in the laminate with multi-angle layers not only relate to its own mechanical property and thickness, but also relate to the mechanical properties of adjacent layers. This phenomenon is so-called "In-situ effect". Hence, the contingency and uncertainty should be considered when determining whether the central 0° ply is fragmented or not. The strength of the 0° ply should be thus revised appropriately according to tensile data.

According to Jalalvand's model [24-25], the modulus of the laminate with randomly saturated fragmentation in the centre 0° ply is given by

$$E_{sat} = E_A \frac{1+\alpha\beta}{\left(1+\beta\right)\left(1+\frac{11}{18}\alpha\beta\right)} \tag{12}$$

Where, α and β are the modulus and thickness ratios between the 0° ply and angle plies in the longitudinal direction, respectively, and E_A is the modulus of the angle plies in the longitudinal direction.

2.6 Failure criteria

Based on the classical laminate theory, the failure of composite laminates generally occurs layer by layer. Therefore, the stress at the first failure of a single layer in the laminate is regarded as the initial failure strength, and the stress at the total failure

of laminate is considered as the ultimate failure strength. In this model, The laminate is considered to fails totally when a single layer is entirely broken for the brittleness property of the fiber. The maximum stress criterion and the Tsai-Hill failure criterion are selected to predict the ultimate failure strength of laminate. For the two-dimensional plane stress condition, the maximum stress criterion for an orthotropic material under tensile load is given by [32]

$$\frac{\sigma_1}{X} \le 1, \quad \frac{|\sigma_2|}{Y} \le 1, \quad \frac{|\tau_{12}|}{S} \le 1 \tag{13}$$

where, X, Y and S represent the strengths in fiber, transverse and in-plane shear directions, respectively. The standard form of the Tsai-Hill failure criterion under two-dimensional plane stress is written as [34]

$$\frac{\sigma_1^2}{X^2} - \frac{\sigma_1\sigma_2}{X^2} + \frac{\sigma_2^2}{Y^2} + \frac{\tau_{12}^2}{S^2} \le 1 \tag{14}$$

Based on the coordinate transformation, Eq. (14) can be rewritten as

$$\sigma_x^2 \left(\frac{\cos^4\theta}{X^2} + \left(\frac{1}{S^2} - \frac{1}{X^2} \right) \cos^2\theta \sin^2\theta + \frac{\sin^4\theta}{Y^2} \right) \le 1 \tag{15}$$

If the stress state is against any one of the two failure criteria, it is considered that the total failure of the laminate occurs. Thus, both the blue and red calculation loops showing in Fig. 1 will be terminated.

3 Model validation

After presenting the analytical model, it is significant to validate the accuracy of the model by comparing the prediction stress-strain curves with the corresponding experimental results. The laminate with $[\pm 25_5]_s$ and $[\pm 25°_5/0°]_s$ layups are manufactured for experimental verification. In addition, the stress-strain curves for laminates with $[\pm\theta_n]_s$ and $[\pm\theta_n/0]_s$ tested by Fuller et al. [1, 16] and Fotouhi et al. [11] are also employed for further assessing the accuracy and adaptability of the analytical model.

3.1 Specimens and tensile experiments

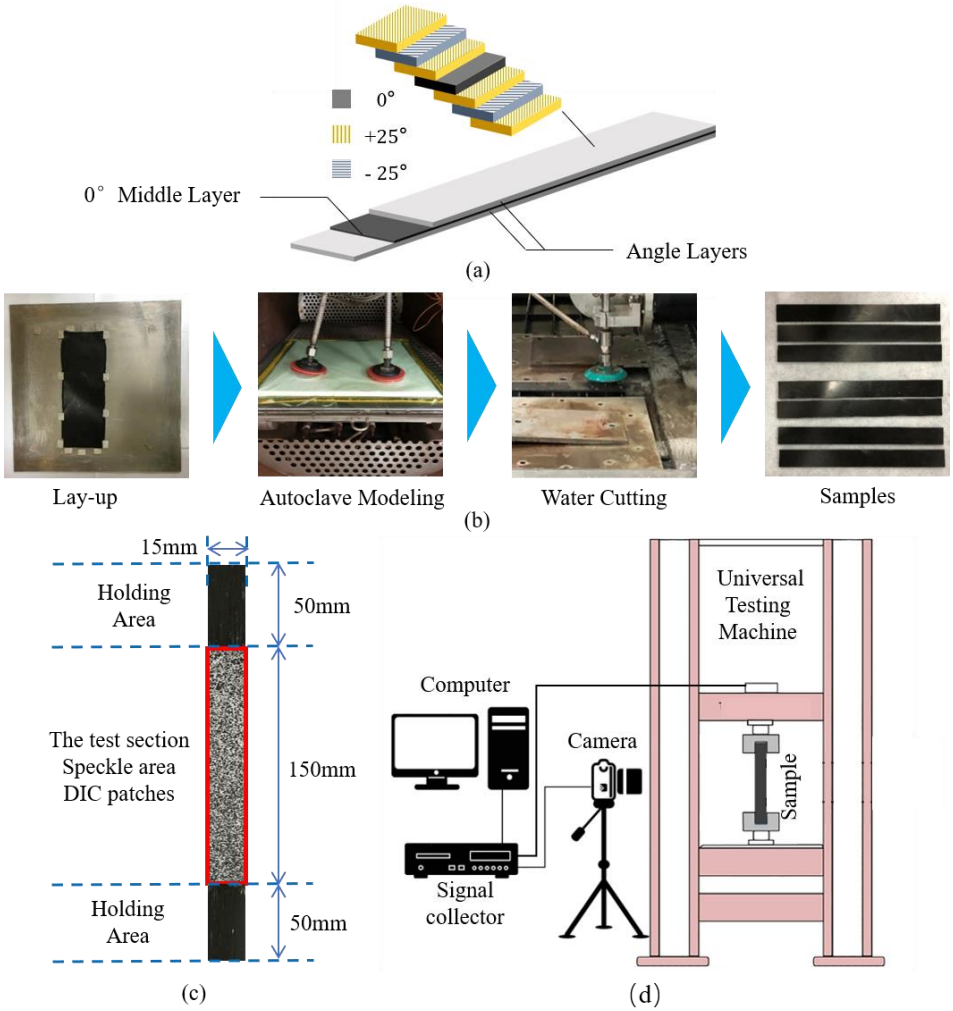

Fig. 3. (a) Stacking structures of the plies for $[\pm 25_5/0]_s$laminate, (b) manufacturing process of the tensile laminate, (c) the shape and size of the tensile specimen, and (d) experimental system for the tensile test.

Thin thermosetting carbon fibre reinforced (CFRP) prepreg, provided by Swancor Advanced Materials Limited Company, is symmetrically stacked to manufacture the laminates with $[\pm 25_5]_s$ and $[\pm 25_5/0]_s$ layups. Stacking pattern and manufacturing procedure are shown in Fig. 3 (a) and (b), respectively. Autoclave forming method is employed to manufacture these laminates. The heating rate is 2℃/min, and the preserved temperature and time are 120 ℃ and 2 hours, respectively. Besides, the vacuum degree is controlled to be greater than 95. After demoulding, a plate with 270 mm (in length) * 100 mm (in width) is prepared. According to the ASTM D 3039 [33], the tensile specimens with the size of 250 mm (in length) * 25 mm (in width) are cut from the laminate plate using water cutting. The schematic diagram of tensile specimens is shown in Fig. 3 (c). All the tensile tests are performed using electronic universal testing machine under displacement control of 2mm/min. The Digital Image

Correlation (DIC) system is used to measure the strain field, shown in Fig. 3 (d). Each kind of test is repeated at least three times to guarantee the generality of the data.

3.2 $[\pm\theta_n]_s$ laminates

The material mechanical properties of the single ply in the laminates manufactured by Swancor prepreg and from Fuller et al. [1] are shown in Table 1. The nonlinear factors of the resin matrix, β_k, are obtained by fitting the stress-strain curves of unidirectional laminates, and the values are shown in Table 2.

Table 1 The mechanical properties of single ply for Swancor and Fuller laminates

	$\boldsymbol{E_1}$ / GPa	$\boldsymbol{E_2}$ / GPa	$\boldsymbol{v_{12}}$	$\boldsymbol{G_{12}}$ / GPa	X / MPa	Y / MPa	S / MPa
Swancor	150	10	0.3	4	850	80	100
Fuller [1]	110	5.2	0.3	2.4	1800	100	150

Table 2 The β_k of ply for Swancor and Fuller laminates

	$\boldsymbol{A_+/A_-}$ layer $\boldsymbol{\beta_1}$ / $\mathbf{Pa^{-3}}$	M layer $\boldsymbol{\beta_1}$ / $\mathbf{Pa^{-3}}$
Swancor	5.5×10^{-14}	6.25×10^{-18}
Fuller et al. [1]	1.2×10^{-15}	5×10^{-18}

Fig. 4. shows the stress-strain behaviour for the Swancor specimens under tensile experiments and the corresponding predictions from the analytical model. The predicted stress-strain curve matches well with the experimental results before the strain of 1.5%. After this strain, the stiffnesses of the three specimens exhibit some difference, while their strengths are approximately identical. Their typical mechanical properties of the specimens are listed in Table 3. The initial modulus is linearly fitted from the stress-strain curve at the strain range of 0.5% to 1%. The symbol "+" and "-" indicate that the predicted value is larger and smaller than the experimental value, respectively. As we can see, compared with the experimental values, all the predicted values of the initial modulus, failure stress and failure strain are bigger. The errors of the initial modulus and failure stress are very small. While, the error of the failure strain is relatively larger, because the failure strain always shows larger divergence than the modulus and strength and is thus more difficult to be predicted well. Even though, we can conclude that the stress-strain curves predicted by the analytical model and from the experiments are in good agreement.

The comparison of the stress-strain curve from Fuller's test [1] and the theoretical prediction is shown in Fig. 5. Three kinds of ply angle, which are 25°, 26° and 27°, are considered. For the laminate of 25° ply angle, the analytical model predicts well the

responses for the entire strain range up to fracture. While regarding the laminates of 26° and 27° ply angles, the analytical model still offers quite good predictions at the strain of less than 2.18%. As the strain increases, the analytical model is seen to slightly overestimate the stresses. All the experimental curves exhibit obvious stiffness degradation after reaching a certain strain, and the analytical model well captures this feature. It can be also seen that, the strain at the onset of nonlinear response increases as the ply angle rise.

The typical mechanical properties of Fuller's laminates are shown in Table 4. The findings reveal that all the predicted values are smaller than the corresponding experimental results, with the error of less than 5%. This implies that the analytical model presents a good prediction on the mechanical behaviours for the Fuller's laminates.

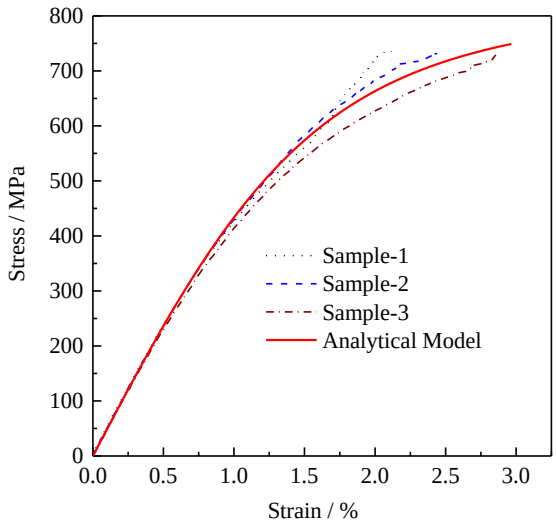

Fig. 4. Comparison of the stress-strain curves tested from the Swancor $[\pm 25_5]_s$ specimens and predicted from the analytical model.

Table 3 Comparison of typical mechanical properties for Swancor specimens

	Initial Modulus / GPa	Failure Stress / MPa	Failure Strain
Sample-1	42.95	720.11	2.117%
Sample-2	43.70	731.93	2.441%
Sample-3	42.02	729.81	2.869%
Average of Tests	42.89	727.28	2.476%
Prediction Value	44.31	749	2.966%
Relative Error	+3.31%	+2.99%	+19.79%

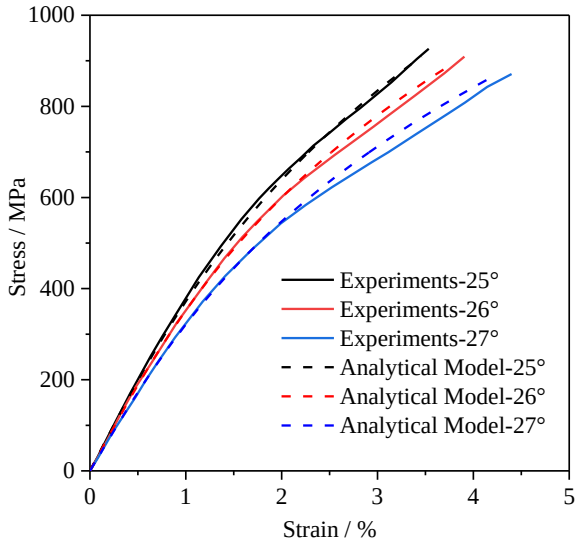

Fig. 5. Comparison of the stress-strain curves from the Fuller's tests and the analytical model

Table 4 Comparison of typical mechanical properties for Fuller laminates

θ	Type	Initial Modulus / GPa	Failure Stress / MPa	Failure Strain
25°	Experiment	35.87	926.35	3.535%
	Prediction Value	34.87	910	3.462%
	Relative Error	-2.79%	-1.76%	-2.06%
26°	Experiment	33.41	909.14	3.907%
	Prediction Value	32.81	886	3.724%
	Relative Error	-1.79%	-2.54%	-4.68%
27°	Experiment	30.55	871.02	4.398%
	Prediction Value	29.95	864	4.192%
	Relative Error	-1.96%	-0.81%	-4.68%

3.3 $[\pm\theta_n/0]_s$ laminates

The stress-strain relation of Swancor laminates, Fuller laminates [16], and Fotouhi laminates [11] are utilized to further validate the accuracy of the analytical model for the $[\pm\theta_n/0]_s$ layering laminates. The material properties of the Swancor laminates are shown in Table 1 and 2, while those of Fuller laminates and Fotouhi laminates are exhibited in Table 5. Both the pure and hybrid carbon fiber laminates are used to validate the analytical model.

Table 5 The mechanical properties of layer for Fuller and Fotouhi laminates

	Fuller	Fotouhi	
	Carbon	Carbon R60	Carbon M50
$\boldsymbol{E_1}$ / GPa	84.4	130	250
$\boldsymbol{E_2}$ / GPa	5.48	4	5
$\boldsymbol{v_{12}}$	0.32	0.3	0.3
$\boldsymbol{G_{12}}$ / GPa	2.37	2	2.4
X / MPa	1900	1500	2100
Y / MPa	500	400	400
S / MPa	400	320	350
$\boldsymbol{\beta}$	5×10^{-18}	1×10^{-16}	5×10^{-17}

Fig. 6. shows a comparison of the stress-strain behavior from the experimental test and the analytical model for Swancor laminates with $[\pm 25_n/0]_s$ layup. Three tests are accomplished to explore the experimental divergence. The mechanical responses of sample 1 and sample 3 show a good consistency, and slight difference of stress is observed after the maximum stress, which is caused by the fragmentation of the middle layer and the thickness effects [25]. While, for the sample 2, it fails before reaching the expected maximum stress. The analytical model is seen to overestimate the stiffness, while the maximum stress predicted by the analytical model is lower than the test data. These differences might be caused by the layup design (the middle layer should be thinner for saturate fragmentation), the manufacture process (gaps and the damage caused by water cutting), and the contingency of the tensile test (The tightness of grips and the verticality of the sample).

The typical mechanical properties for Swancor laminates are presented in Table 6. Compared with the experimental values, it is found that the relative errors for initial modulus, maximum stress and failure stress are +1.58%, -7.66% and +4.84%, respectively, which demonstrates the good predictability of the analytical model. While, for the failure strain and the strain at the maximum stress, the analytical model underestimates these values with relatively larger errors.

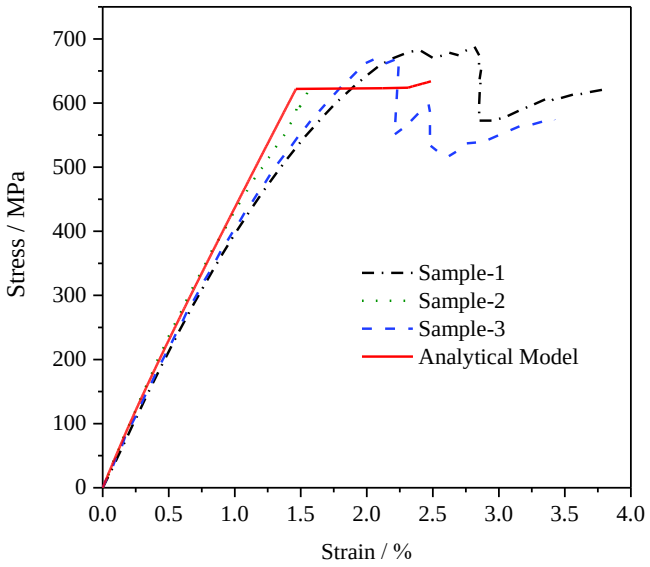

Fig. 6. Comparison of the stress-strain curves tested from the Swancor $[\pm 25_5/0]_s$ laminates and predicted from the analytical model.

Table 6 Comparison of typical mechanical properties for Swancor laminates

	Initial Modulus / GPa	Maximum Stress / MPa	Strain at Maximum Stress	Failure Stress / MPa	Failure Strain
Sample-1	41.76	680.23	2.336%	620.56	3.781%
Sample-2	45.42	---	---	619.95	1.549%
Sample-3	42.12	667.01	2.023%	573.65	3.365%
Average Value	43.1	673.62	2.179%	604.72	2.898%
Prediction Value	43.78	622	1.464%	634	2.486%
Relative Error for Average	+1.58%	-7.66%	-32.81%	+4.84%	-14.22%

Fig. 7. exhibits the stress-strain curve of Fuller laminates. The analytical model can well predict the tensile response, such as the elastic behaviors and the slight stiffness degeneration before the plateau stress. The stiffness degeneration results from the progressive damage of each layer and the fibre rotating. In addition, the predicted onset point of the plateau stress has a good consistency with the test values. However, the length of the predicted plateau stage is seen to be shorter than those of tests. The predicted stiffness after the plateau stage is higher than those of tests. This may result from that the in-situ effect of each layer changes the overall stiffness response and the middle layer shows negligible influence on the surrounding layer after its fragmentation.

Even though, it can be concluded that the stress-strain behaviors predicted by the analytical model and tested from the experiments are in good agreement.

The typical mechanical properties for Fuller laminates are exhibited in Table 7. It is found that, except for the failure stress, the relative errors for these considered properties are less than 10%. The relatively larger errors of failure stress may be caused by accuracy of failure criterion, sample defects and individual specificity. The predicted failure strain is smaller than the tested values, which may be caused by the idealization of the analytical model in dealing with fragmentation within a layer. The analytical model considers that the fibers exhibit uniform multi-points fracture entirely. But, in fact, the real damage consists of fiber pull out, random multi-points fiber fracture or even incomplete fracture, which result in larger strain. Based on the results of $[\pm\theta_n/0]_s$ laminates, it can be concluded that the analytical model has acceptable prediction accuracy and high effectiveness about the mechanical response.

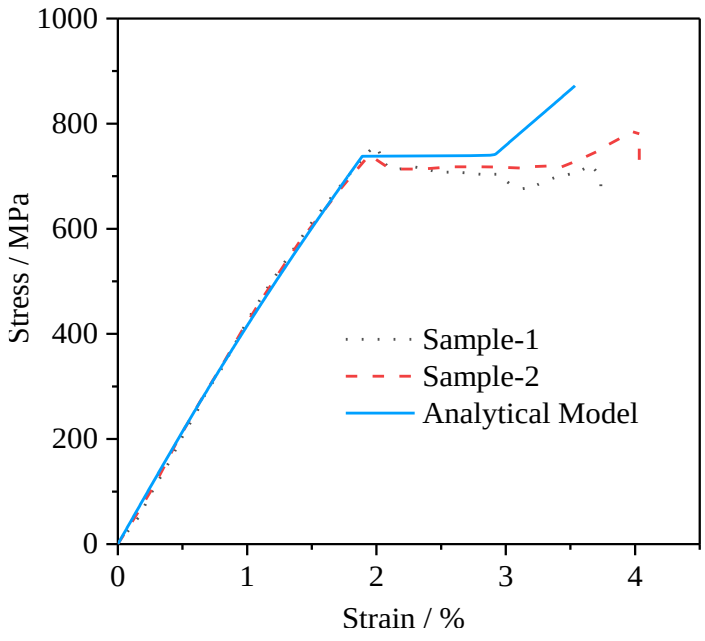

Fig. 7. S omparison of the stress-strain curves from the Fuller's tests and the analytical model.

Table 7 Comparison of typical mechanical properties of Fuller laminates

	Initial Modulus / GPa	Onset Stress of Plateau Stage / MPa	Onset Strain of Plateau Stage	Failure Stress / MPa	Failure Strain
Sample-1	43.29	760.08	1.996%	719.76	3.736%
Sample-3	41.55	739.32	1.969%	790.32	4.032%
Average	42.42	727.28	1.983%	749.70	3.884%
Prediction Value	40.36	738	1.892%	872	3.536%
Relative Error	-4.86%	-1.56%	-4.59%	+15.49%	-8.96%

Fig. 8 shows the stress-strain curve for Fotouhi interlayer hybrid composite laminates. It is clearly shown that the mechanical response and the stiffness change of laminates before the plateau stage is well predicted by the analytical model. In addition, the onset stress of the plateau stage is also well predicted by the analytical model. However, no obvious platform is observed from the experimental results. When the strain is larger than 1.4%, the stiffness of the test curve degenerates faster than the prediction of the analytical model. This indicates that there may be other progressive damage modes apart from the modes that the analytical model considers, like the progressive stable delamination. While, this phenomenon needs to be further studied.

The typical parameters of Fotouhi hybrid fiber laminates are shown in Table 8. The initial modulus is fitted from the stress-strain relation at the strain range of 0.25%~0.75%. Apart from the failure strain, the relative errors of the mechanical properties are all within 10%. Even though, the relative error of the failure strain are higher, it is still within an acceptable accuracy range. Therefore, the analytical model still has the acceptably well prediction accuracy for interlayer hybrid laminates with $[\pm\theta_n/0]_s$ layup.

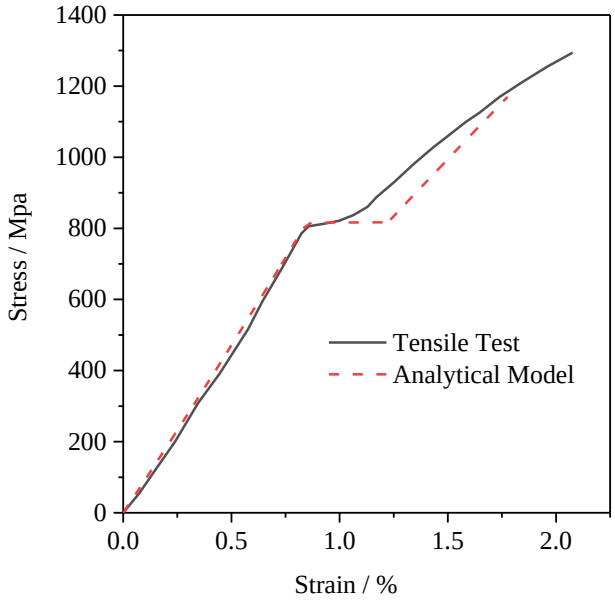

Fig. 8. Comparison of the stress-strain curves from the Fotouhi's tests and the analytical model.

Table 8 Comparison of typical mechanical properties of Fotouhi laminates

	Initial Modulus / GPa	Onset Stress of Plateau Stage / MPa	Onset Strain of Plateau Stage	Failure Stress / MPa	Failure Strain
Experiment	98.48	805.59	0.857%	1294.41	2.077%
Prediction Value	97.08	816	0.848%	1170	1.776%
Relative Error	-1.42%	+1.29%	-1.05%	-9.61%	-14.49%

The results reveal that the analytical model can give good predictions on the tensile nonlinear response for the $[\pm\theta_n]_s$ laminates, and pure and hybrid fiber laminates with $[\pm\theta_n/0]_s$ layup. Therefore, this analytical method can be used as a straightforward design tool for laminates.

4 Parameter sensitivity analysis

After verifying the accuracy of the analytical model, it is necessary to study the sensitivity of the model parameters on the mechanical responses. The two kinds of laminates with $[\pm\theta_n]_s$ layup (i.e., Swancor laminate and Fuller laminate) are selected as the examples for analysis. The variation tendency of the failure strain is used to describe the parameter sensitivity of the model. The tensions are applied to the samples with different layering angles. We preserve the other model parameters while changing the dominated parameter. Fig. 9 and 10 illustrates the variations of the failure strain

according to change of model parameters for the samples of different layering angles.

When the layering angle is 0°, shown in Fig. 9 (a), the failure strain is most sensitive to E_1, while insensitive to others. This obeys the common sense for unidirectional continuous fiber laminates under tension. For 10° layering angle, shown in Fig. 9 (b), E_1 and G_{12} are two dominated parameters for the failure strain. Furthermore, the influence of G_{12} gradually becomes stronger than that of E_1. Fig. 9 (c) shows the behavior of the laminates with 15° layering angle. As can be seen, the G_{12} is the most sensitive parameter for failure strain, followed by E_1. The influence of other parameters is negligibly small.

According to the shear nonlinearity given by equation (6), the nonlinear factor of resin matrix indirectly affects the stiffness by adjusting the value of S_{66}. So, the sensitivity of the β_k positively correlates to the G_{12}. For the layering angle of 25°, shown in Fig. 9 (d), the failure strain is most sensitive to the G_{12}, and is thus sensitive to β_1 (nonlinear factor for A_+/A_- layers) and β_2 (nonlinear factor for *C* layers). However, the effect of β_1 and β_2 on the failure strain is opposite, which implies that the failure strain increases with increasing β_1, while decreasing β_2. Besides, the failure strain is more sensitive on β_1 than β_2, and the effect of the β_2 can be even ignored when the matrix interface is thinner. For the laminates with 30° and 35° layering angle, their behaviors are similar to that of 25° layering angle, as shown in Fig. 9 (e) and (f). The dominant sensitive parameters are also G_{12}, β_1 and β_2, and the E_2 gradually shows its influence on the failure strain.

The main tendency for the 40° layering angle is resemblance to that of angle 35° as shown in Fig. 10 (a), and the E_2 is more dominant than the β_1. For the 45° layering angle (Fig. 10 (b)), the E_2 becomes the most sensitive parameters. Meanwhile, the effect of the nonlinear factors on the failure strain is linear. Regarding the 90° layering angle (Fig. 10 (c), the E_2 becomes the dominant parameter to the failure strain.

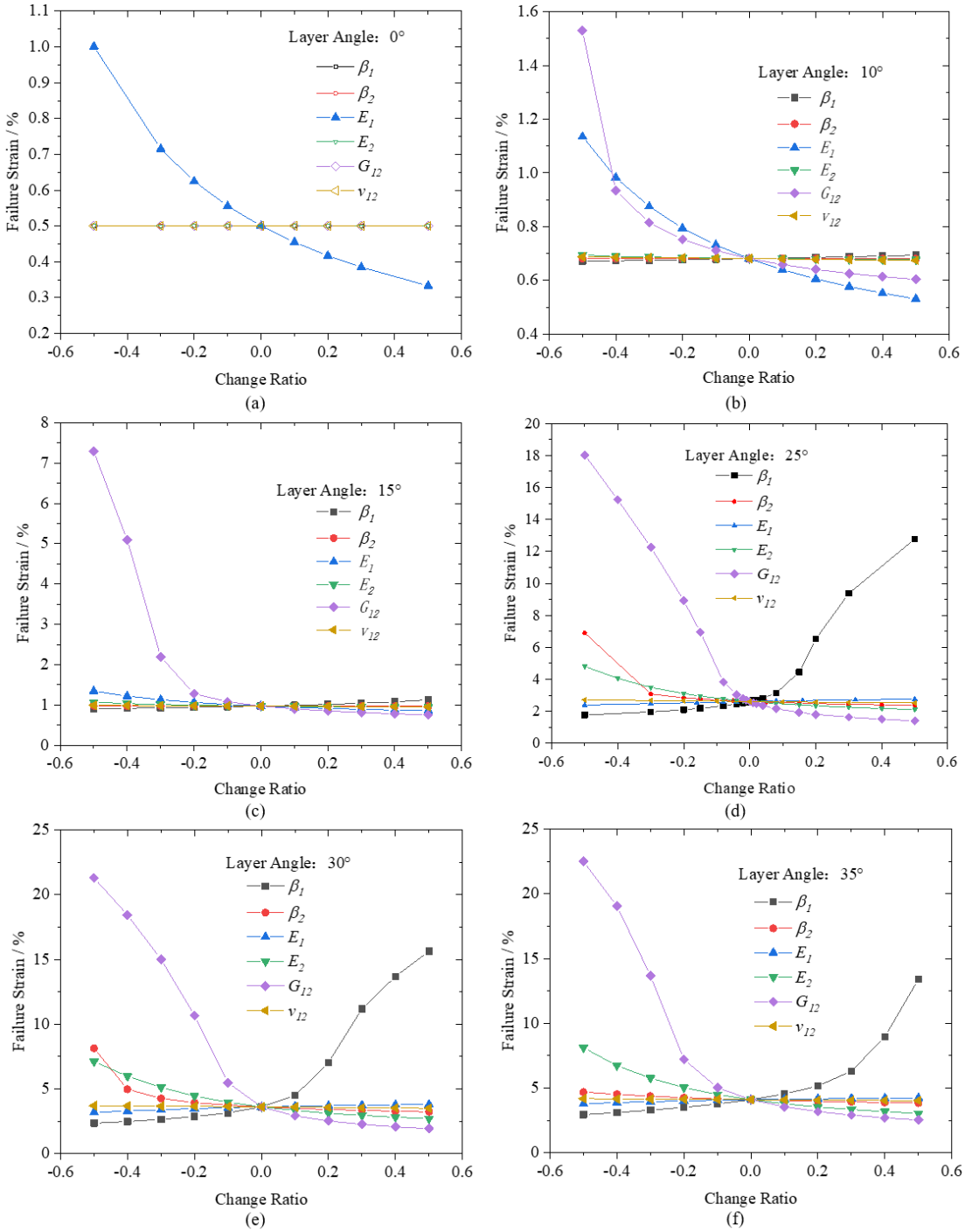

Fig. 9. The variation of failure strain on the model parameters for the $[\pm\theta_n]_s$ Swancor laminate at the layering angle of (a) 0°, (b) 10°, (C) 15°, (d) 25°, (e) 30° and (f) 35°.

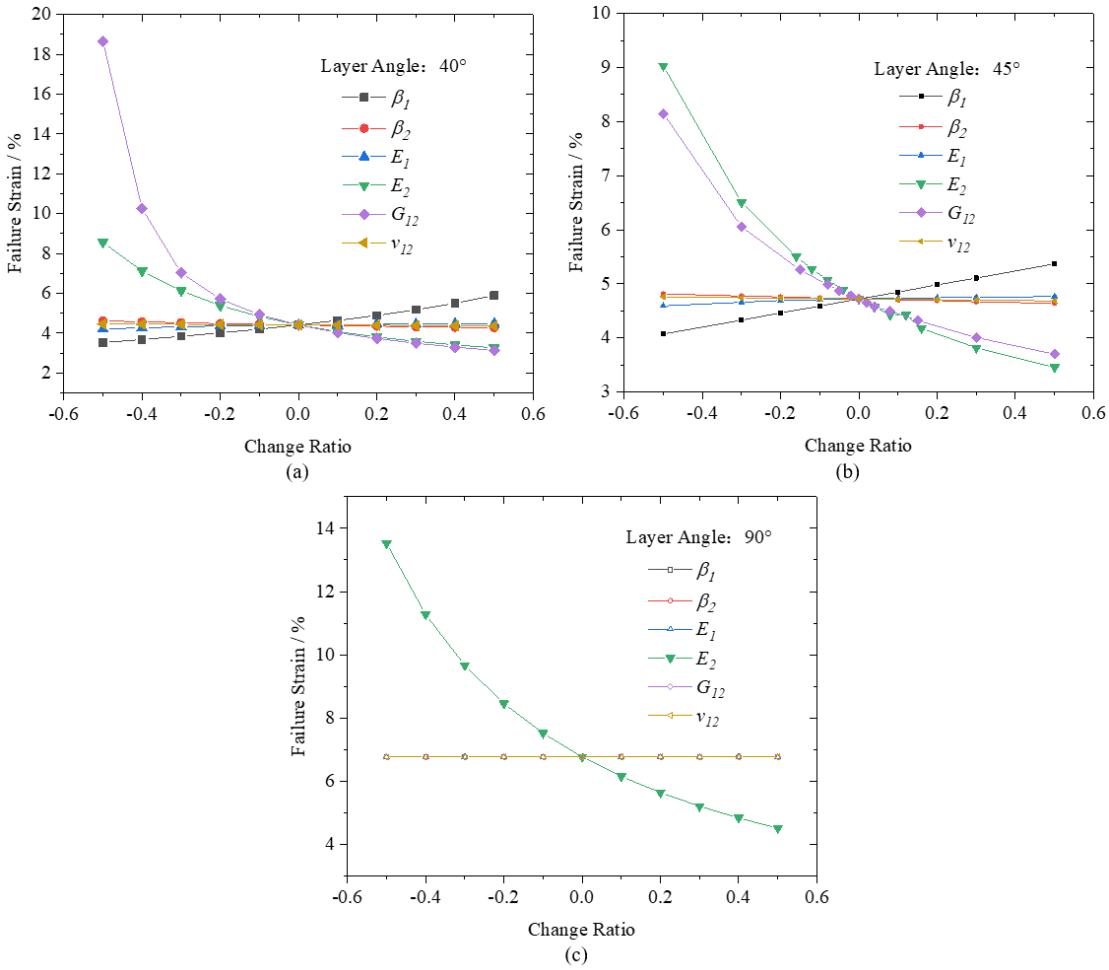

Fig. 10. The variation of failure strain on the model parameters for the $[\pm\theta_n]_s$ Swancor laminate at the angle of (a) 40°, (b)45° and (c) 90°.

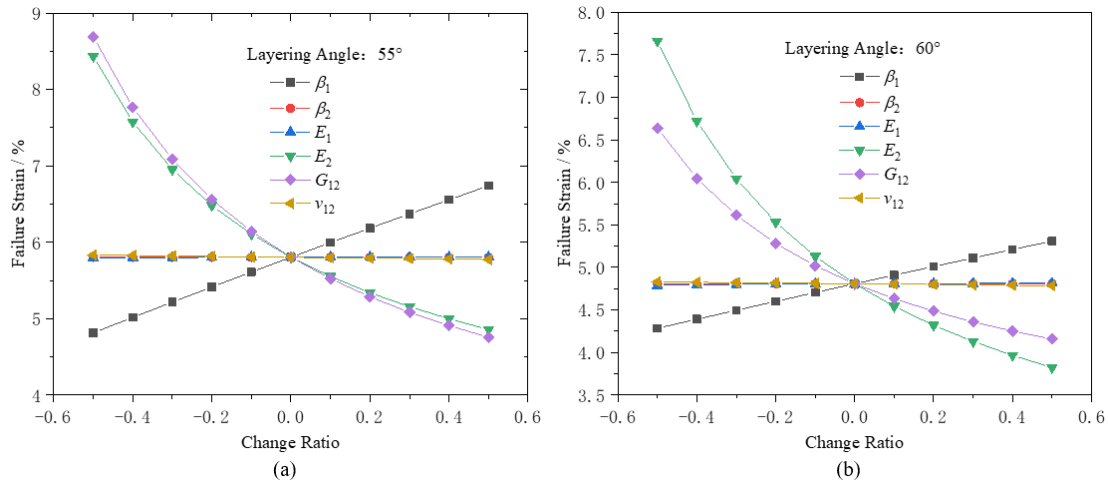

Fig. 11. The variation of failure strain on the model parameters for the $[\pm\theta_n]_s$ Fuller laminate at the angle of (a) 55° and (b) 60°.

The findings of sensitivity analysis reveal that the dominantly sensitive model

parameter changes from E_1 to G_{12}, and finally to E_2 as the ply angle increases from 0° to 90°. Comparing Fig.10 (a) and (b) with Fig. 11 (a) and (b), it is found that the layering angle is different for different materials at which the most sensitive parameter changes from G_{12} to E_2. Furthermore, the failure strain is more affected by the β_1 than β_2, and the effect of β_2 is usually omitted in $[\pm\theta_n/0]_s$ laminates for composite design.

5 Conclusion

In this paper, a novel analytical model for laminates with $[\pm\theta_n]_s$ and $[\pm\theta_n/0]_s$ layup is established, and its prediction accuracy is validated experimentally. In addition, sensitivity analysis of the model parameters is also carried out. Some conclusions are summarized as follows:

(a) The analytical model combines the mechanism of fiber rotation, shear nonlinearity, progressive failure and fragmentation to describe the nonlinear behaviors of the laminates. This model can capture well most mechanical properties, including the stiffness degradation, initial modulus, onset stress of plateau stage and maximum tress. But for the failure stress and failure strain, the failure criteria need to be improved to give more accurate prediction.

(b) The analytical model can well predict the mechanical behaviors for both the progressive and instant decreases of the stiffness, with regard to laminates with $[\pm\theta_n]_s$ layup, pure fiber laminates with $[\pm\theta_n/0]_s$ layup and interlayer hybrid laminates with $[\pm\theta_n/0]_s$ layup. However, according to test for laminates with $[\pm25_5/0]_s$ layup, the prediction show some differences compared to test because of the thickness effect, though the transient decrease of stiffness is well predicted.

(c) For the sensitivity analysis of the model parameters, the dominant sensitive parameter changes from E_1 to G_{12}, and finally to E_2 as the ply angle increases from 0° to 90°.

Reference

[1] Fuller J, Wisnom M R. Exploration of the potential for pseudo-ductility in thin ply CFRP angle-ply laminates via an analytical method[J]. Composites Science and Technology, 2015, 112: 8-15.

[2] Swolfs Y, Gorbatikh L, Verpoest I. Fibre hybridization in polymer composites: A review[J]. Composites Part A: Applied Science and Manufacturing, 2014, 67: 181-200.

[3] Zweben C. Tensile strength of hybrid composites[J]. Journal of Materials Science, 1977, 12(7): 1325-1337.

[4] Manders P W, Bader M G. The strength of hybrid glass/carbon fibre composites - Part 2: A statistical model[J]. Journal of Materials Science, 1981, 16 (8): 2246-2256.

[5] Hedgepeth, J M. Stress concentrations in filamentary structures[R]. NASA TN, 1961: 1-36.

[6] Tang J, Swolfs Y, Yang M, et al. Discontinuities as a way to influence the failure mechanisms and tensile performance of hybrid carbon fiber/self-reinforced polypropylene composites[J]. Composites Part A: Applied Science and Manufacturing, 2018: 354-365.

[7] Tang J, Swolfs Y, Aslani A, et al. Engineering tensile behavior of hybrid carbon fiber/self-reinforced polypropylene composites by bio-inspired fiber discontinuities[J]. Composites Part B: Engineering, 2019: 107502.

[8] Szebényi G, Magyar B, Czigany T. Achieving Pseudo-Ductile Behavior of Carbon Fiber Reinforced Polymer Composites via Interfacial Engineering[J]. Advanced Engineering Materials, 2021, 23: 2000822.

[9] Yuan Y, Wang S, Yang H. Analysis of pseudo-ductility in thin-ply carbon fiber angle-ply laminates[J]. Composite Structures, 2017, 180: 876-882.

[10] Yu H N, Longana M L, Jalalvand M, et al. Hierarchical pseudo-ductile hybrid composites combining continuous and highly aligned discontinuous fibers[J]. Composites Part A: Applied Science & Manufacturing, 2017, 105: 40-56.

[11] Fotouhi M, Jalalvand M, Wisnom M R. High performance quasi-isotropic thin-ply carbon/glass hybrid composites with pseudo-ductile behaviour in all fibre orientations[J]. Composites Science and Technology, 2017, 152: 101-110.

[12] Czél G, Ver T, Jalalvand M, et al. Pseudo-ductility and reduced notch sensitivity in multi-directional all-carbon/epoxy thin-ply hybrid composites[J]. Composites Part

A: Applied Science and Manufacturing, 2018, 104: 151-164.

[13] Jalalvand M, Czel G, Wisnom M R. Reducing the notch sensitivity of quasi-isotropic layups using thin-ply hybrid laminates[C]. Proceedings of the American Society for Composites - 30th Technical Conference, ACS 2015 American Society for Composites.

[14] Hassani F, Martin P J, Falzon B G. Progressive failure in inter-ply hybrid composites of self-reinforced polypropylene and glass fibre[J]. Polymer, 2020, 195: 122411.

[15] Selezneva M, Swolfs Y, Katalagarianakis A, et al. The brittle-to-ductile transition in tensile and impact behavior of hybrid carbon fibre/self-reinforced polypropylene composites[J]. Composites Part A: Applied Science and Manufacturing, 2018, 109: 20-30.

[16] Fuller J D, Jalalvand M, Wisnom M R. Combining fibre rotation and fragmentation to achieve pseudo-ductile CFRP laminates[J]. Composite Structures, 2016, 142: 155-166.

[17] Jalalvand M, Fotouhi M, Wisnom M R. Orientation-dispersed pseudo-ductile hybrid composite laminates - A new lay-up concept to avoid free-edge delamination[J]. Composites Science and Technology, 2017, 153: 232-240.

[18] Fotouhi M, Jalalvand M, Wisnom M R. Notch insensitive orientation-dispersed pseudo-ductile thin-ply carbon/glass hybrid laminates[J]. Composites Part A: Applied Science and Manufacturing, 2018, 110: 29-44.

[19] Alessi R, Ciambella J, Paolone A. Damage evolution and debonding in hybrid laminates with a cohesive interfacial law[J]. Meccanica, 2017, 52: 1079-1091.

[20] Zhuang W, Ao W. Effect of stacking angles on mechanical properties and damage propagation of plain-woven carbon fiber laminates[J]. Materials Research Express, 2018, 5(3): 035603.

[21] Fotouhi M, Jalalvand M, Saeedifar M, et al. High performance quasi-isotropic thin-ply carbon/glass hybrid composites with pseudo-ductile behaviour loaded off-axis[J]. Composite Structures, 2020, 247: 112444.

[22] Ebrahimnezhad-Khaljiri H, Eslami-Farsani R, Akbarzadeh E. Effect of interlayer hybridization of carbon, Kevlar, and glass fibers with oxidized polyacrylonitrile fibers on the mechanical behaviors of hybrid composites[J]. Proceedings of the Institution of Mechanical Engineers Part C: Journal of Mechanical Engineering Science, 2019, 234(9): 1823-1835.

[23] Pozegic T R, Fotouhi M, Wu X, et al. Pseudo-ductile behaviour in fibre reinforced

thermoplastic angle-ply composites[J]. Composites Science and Technology, 2020, 197: 108261.

[24] Jalalvand M, Czél G, Wisnom M R. Numerical modelling of the damage modes in UD thin carbon/glass hybrid laminates[J]. Composites Science and Technology, 2014, 94: 39-47.

[25] Jalalvand M, Czél G, Wisnom M R. Damage analysis of pseudo-ductile thin-ply UD hybrid composites – A new analytical method[J]. Composites Part A: Applied Science and Manufacturing, 2015, 69: 83-93.

[26] Hahn H T, Tsai S W. Nonlinear elastic behavior of unidirectional composite laminae[J]. Journal of Composite Materials, 1973, 7(1): 102–18.

[27] Wisnom MR. The effect of fibre rotation in 45 tension tests on measured shear properties[J]. Composites, 1995, 26: 25–32.

[28] Fuller JD, Wisnom MR. Pseudo-ductility and damage suppression in thin ply CFRP angle-ply laminates[J]. Composites Part A: Applied Science and Manufacturing, 2014, 69: 64–71.

[29] Goyal V K, Jaunky N R, Johnson E R, et al. Intralaminar and interlaminar progressive failure analyses of composite panels with circular cutouts [J]. Composite Structures, 2004, 64(1): 91-105.

[30] Hu H T, Lin W P. Nonlinear Analysis of Fiber-Reinforced Composite Laminates Subjected to Uniaxial Tensile Load[J]. Journal of Composite Materials, 2002, 36: 1429.

[31] Hu H T, Lin F M, Liu H T, et al. Constitutive modeling of reinforced concrete and prestressed concrete structures strengthened by fiber-reinforced plastics[J]. Composite Structures, 2010, 92(7): 1640-1650.

[32] Hu HT, Lin WP, Tu FT. Failure analysis of fiber-reinforced composite laminates subjected to biaxial loads[J]. Composites Part B: Engineering, 2015, 83: 153-165.

[33] Astm D. Standard Test Method for Tensile Properties of Polymer Matrix Composite Materials[J]. 2008.

[34] S.W. Tsai. Strength theories of filamentary structures. New York: Wiley Interscience, Fundamental aspects of fiber reinforced plastic composites[C]. 1968: 3–11.